THE PENNSYLVANIA STATE UNIVERSITY
SCHREYER HONORS COLLEGE

DEPARTMENT OF ENGINEERING SCIENCE AND MECHANICS

DESIGN AND CONTRUCTION OF LOW FIELD EDMR SPECTROMETER

COLIN G. MCKAY
SPRING 2014

A thesis
submitted in partial fulfillment
of the requirements
for a baccalaureate degree
in Engineering Science
with honors in Engineering Science

Reviewed and approved* by the following:

Patrick M. Lenahan
Distinguished Professor of Engineering Science and Mechanics
Thesis Supervisor

Barbara A. Shaw
Professor of Engineering Science and Mechanics
Honors Adviser

Judith A. Todd
P.B. Breneman Department Head Chair
Professor, Department of Engineering Science and Mechanics

* Signatures are on file in the Schreyer Honors College.

ABSTRACT

Low k dielectric materials are the future of large scale integrated circuits; however unknown defects and imperfections are inhibiting these devices by preventing them from reaching their optimal performance. The purpose of this work is to design and construct a low field Helmholtz Coil Electrically Detected Magnet Resonance spectrometer for use on low k dielectric materials to better understand these defects. The magnet is composed mainly of aluminum with several thousand feet of enamel coated copper magnet wire. This paper explains most of the design process and construction procedures as well as the design flaws which could have rendered the magnet useless and the fixes to those problems. The final product of this work is a fully working, high fidelity, uniform magnetic field EDMR spectrometer which shows a lot of promise for future research on low k dielectric materials. Experiments carried out on silicon carbide based MOSFETs show a very good zero-field signal to noise ratio. I look forward to my future work using this spectrometer.

TABLE OF CONTENTS

List of Figures iii

Chapter 1 Introduction 1

- Problem Statement 1
- Design Needs 2
- Objectives 2

Chapter 2 Literature Review 3

- Defects in Semiconductor Devices 3
- Defect Characterization via EDMR and ESR Techniques 8
- Low Field/Zero Field Measurements in Full Devices 9
- Helmholtz Coil Design 10

Chapter 3 Helmholtz Coil Design Process 12

- MATLAB Code 12
- CAD Modeling 13
- Building Techniques 15
  - Fabrication of Structural Frame 15
  - Spun by hand 16
  - Spun on ring stand 16
- Problems Encountered and Fixes 16

Chapter 4 Design Validation 20

- Zero-Field Signal 20

Chapter 5 Results and Discussions 23

Chapter 6 Conclusions 25

Appendix A MATLAB Code 26

Appendix B AUTODESK Inventor Models and Final Product 28

BIBLIOGRAPHY 30

LIST OF FIGURES

Figure 2-1: Variable Range Hopping Band Diagram 3

Figure 2-2: TDDB Leakage Current vs. Time 5

Figure 2-3: Deep defects (a) allow for more electron tunneling than shallow defects (b).....6

Figure 2-4: Pre and post stressing oxide states 7

Figure 2-5: Energy difference between spin states 8

Figure 3-1: Helmholtz Coil Locations 12

Figure 3-2: Magnet Assembly with T-holder 14

Figure 4-1: Modulation Coil Circuit Diagram 21

Figure 4-2: First Zero Field Resonance Signal 22

Figure 5-1: Silicon Carbide Transistor Zero-Field Signal 24

Figure 8-1: Magnet CAD Model Full Assembly 28

Figure 8-2: Magnet CAD Model Assembly with Cold Finger and T 28

Figure 8-3: Completed Wired Magnet 29

Figure 8-4: Experimental Setup 29

Chapter 1

Introduction

Problem Statement

The performance of integrated circuits can be improved by introducing low dielectric constant materials as interlayer dielectrics. There are several problems with these low dielectric constant insulating materials that are not yet very well understood. These problems include but are not limited to time dependent dielectric breakdown (TDDB), variable range hopping (VRH), negative bias temperature instability (NBTI), and stress induced leakage currents (SILC). These problems can be caused by various defects in the interlayer dielectric in a metal oxide semiconductor field effect transistor (MOSFET) integrated circuits. The purpose of this thesis project is to design a low field/zero-field Helmholtz coil based electromagnetic resonance spectrometer to carry out electrically detected magnet resonance (EDMR) experiments. These EDMR measurements will hopefully shed some light on the physics behind these problems.

This project has real potential technological significance. The MOSFET is the basic device that all logic processors such as computer chips use to "make decisions". Computer chips have gotten faster over the years as the devices have gotten smaller. To make them even faster, new materials with lower dielectric constants have been introduced into the design to lower the RC time constant of the chip which in turn increases the speed of the device. Although these lower capacitance materials aid in the theoretical response time of these chips, there are performance inhibiting defects that prevent the devices from reaching their theoretical capabilities. Some of these defects can cause catastrophic failures such as TDDB and prevents the devices from being considered reliable enough for commercial use.

Design Needs

Electron spin resonance (ESR) and EDMR are two very powerful tools used to better understand the types of defects that cause the problems stated above. The focus of this work will be to design a low field EDMR spectrometer composed of 3 sets of progressively larger Helmholtz coils with a fourth set of smaller "modulation coils". EDMR can use a smaller magnetic field than ESR which requires a very large magnetic field. The design of the coils will need to be optimized for the power source available to ensure that the maximum field is achievable for the length of wire that will be used. This will be an iterative process through calculations performed in MATLAB.

In order to provide a reasonably complete EDMR response, the Helmholtz coils will have to achieve a maximum uniform field of around 150 Gauss in the sample region. The Helmholtz coil frame will also have to be capable of dissipating around 100 Watts of resistive heating power while the magnet is operating. The main frame must be made of non-magnetic materials (mostly aluminum) so as to not interfere with the uniformity of the field created by the coils. Another major design constraint is the strength of aluminum under the mechanical load of the coils' weight. Aluminum is not as strong as steel and the shape of the support structures will have to be taken into account during the design process.

Objectives

The goal of this project is to design and build a fully working low field EDMR spectrometer. The field produced will have to be quite consistent, accurate, and reproducible to ensure that the results are meaningful. The current dependence of the field produced by the coils must be well understood because the computer software that will run the spectrometer will assume an applied magnetic field as a function of the known current flowing through the coils. If these characteristics are not well understood the measurements would turn out to be useless.

Chapter 2

Literature Review

Defects in Semiconductor Devices

MOSFETs have always had defects in their structures for as long as they have been built. These defects have not always been a terrible problem but as the size of these devices gets smaller, the effect of these defects gets bigger. When MOSFETs were first being built by Bell Laboratories, these devices were large enough to fit comfortably in your hand. Nowadays these transistors have a nominal gate length of about 22 nanometers. (Bohr, 2014) The fairly small number of defects that had little to no effect on the large devices drastically affects the performance of these smaller devices via trapping and tunneling of electrons.

VRH is one of the problems encountered in small devices in which a defective dielectric material allows enough electrons to travel through it to be considered conductive. These electrons tunnel from defect to defect inside the dielectric material until they reach the other side. Since these dielectrics were meant to prevent charge carriers from crossing that space, a dielectric that allows for tunneling severely inhibits the performance of a device. The band diagram of this material would be idealized to look like Figure 2-1.

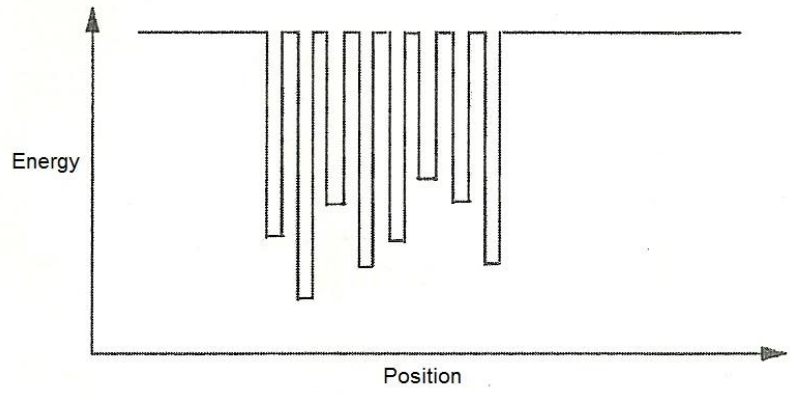

Figure 2-1: Variable Range Hopping Band Diagram

Variable range hopping is an activated tunneling process. The three main parameters that determine variable range hopping are a frequency which is dependent on phonons in the structure, an Arrhenius temperature dependence, and a tunneling model. All three of these must be taken into account when trying to think about variable range hopping. Sir Neville Mott went through the math and determined that the only defects worth considering in the structure were those within about $2k_BT$ (where k_B is the Boltzmann constant and T is the absolute temperature in Kelvin) because below these energy levels there would be almost no unoccupied states, and at the higher end of the spectrum, it would require too much energy for an electron to tunnel into an energy state significantly higher than its own energy. After all of Mott's calculations, he came to the conclusion that VRH is a fairly ohmic process at low electric fields and that is scales with an exponential of the reciprocal of the one-fourth power of the temperature. (Mott, 1987)

Another problem associated with defects in MOS devices is TDDB in which a dielectric material operating at electric fields below its breakdown field will suddenly fail catastrophically without warning. This phenomenon is still not wholly understood but it is believed that electron tunneling plays a role. TDDB is a problem found in a very wide variety of systems.

What is known about TDDB is that a dielectric material under normal operating conditions, in which the applied field is below the breakdown field, fails as if the device were to undergo breakdown and act as a short instead of an insulator. This problem has become more prominent as thinner low-k dielectric materials have been introduced to maintain the continued scaling down of very large scale integrated circuits such as computer processor chips. The problem becomes more pronounced with the ultra-low-k materials needed for use in new high speed integrated circuits.

Measuring the leakage current through a dielectric material over time shows that in many cases, the leakage current actually initially starts to decrease for a time before the insulator starts to conduct large amounts of current through a region that was supposed to be electrically

insulated. This can be seen in Figure 2-2 taken from Chen (2009) where the leakage current spikes at the moment of time dependent dielectric breakdown.

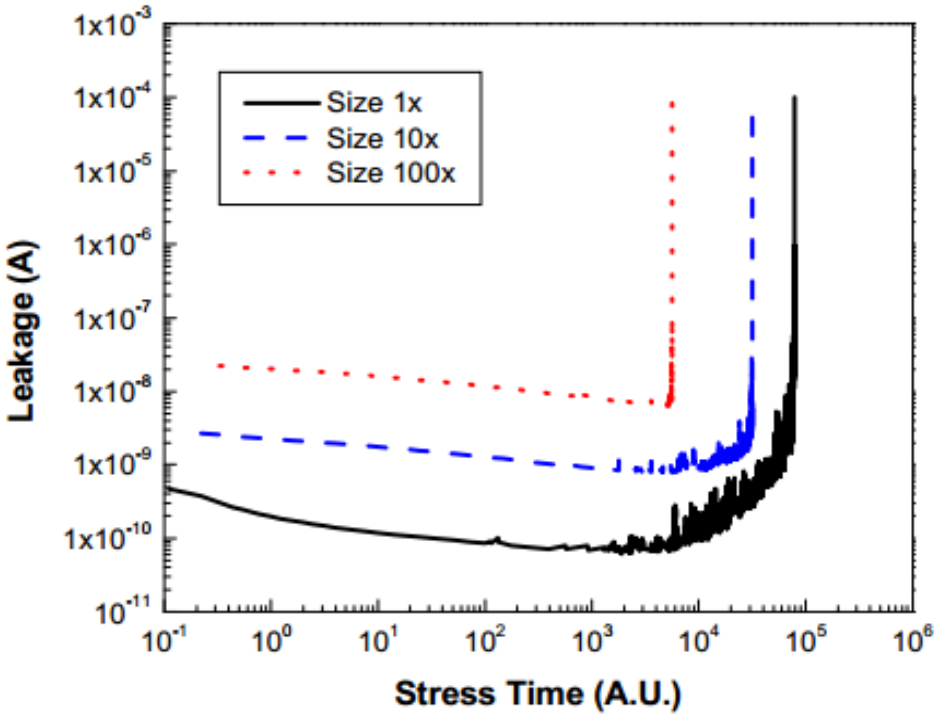

Figure 2-2: TDDB Leakage Current vs. Time

There are several models that try to explain the phenomenon of TDDB. The main models are the E and the 1/E theories. The E model states that the time to failure is proportional to an exponential involving a field dependent activation energy:

$$\ln(TF) \propto \left(\frac{\Delta H_{0-}\gamma E_{ox}}{k_b T}\right)$$

where ΔH_0 is the activation energy required for breakdown, E_{ox} is the applied electric field in the oxide, $k_b T$ is the product of the Boltzman constant and absolute temperature, and $\gamma$is the field acceleration parameter. (McPherson, 1998) The 1/E model follows many of the same parameters of the E model but instead relies on a $1/E_{ox}$ term instead of the E_{ox} dependence.

Several studies have been carried out which show that for low field thin dielectrics, the E model serves as a better fit to the data than the 1/E model. (McPherson, 1998) As stated earlier, it seems that electron tunneling is an important part of TDDB and one theory is that as electrons fill deep level defects within the oxide they eventually create a conductive channel through the insulator. This was determined by analyzing the levels of defects in the oxides to find that TDDB under bias temperature stresses were more common for oxides with deep level defects at or near the Fermi level of the semiconductor while shallow defects significantly above the Fermi level were not as susceptible to TDDB and tunneling. This is clearly demonstrated in Figure 2-3. (Miyazaki et al, 2009)

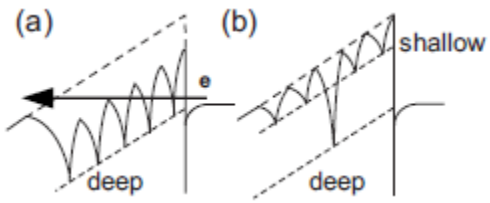

Figure 2-3: Deep defects (a) allow for more electron tunneling than shallow defects (b)

Yet another problem that plagues MOS integrated circuits is the negative bias temperature instability (NBTI). This problem mostly affects p-channel MOSFET devices. The effects of NBTI include unstable changes to threshold voltage of a device from both interface states and oxide space charge. (Lenahan, 2010)

NBTI causes large device performance problems as the oxide space charge grows and oxide-semiconductor interface states interfere with the conductive channel. These problems make devices unreliable as the threshold voltage for the devices changes over time. NBTI also reduces transistor switching speed.

It is believed that NBTI is caused by hydrogen passivated silicon dangling bonds being freed during stressing of the oxide. When an oxide is stressed the silicon bonds in the oxide (due to an missing oxygen) can break leaving a silicon dangling bond in the oxide. Although all of the dangling bonds at the interface have been passivated by a hydrogen anneal, the large number of broken bonds in the oxide and the "perfect" passivated interface layer is not thermodynamically stable as the Gibbs free energy is not at its lowest possible value due to the lack of entropy. The entropy is significantly increased when some of the hydrogen atoms that were used to passivate the interface layer move into the oxide creating unpassivated interface states. The overall charge in the oxide which grows due to broken bonds as well as the creation of interface states increases the voltage required at the gate to turn on the device. This unreliable and growing threshold voltage gives rise to NBTI. The pre and post stressing states are shown in Figure 2-4 (Lenahan, 2007) where the post stressing state would be more thermodynamically stable is some of the hydrogens moved up into the oxide.

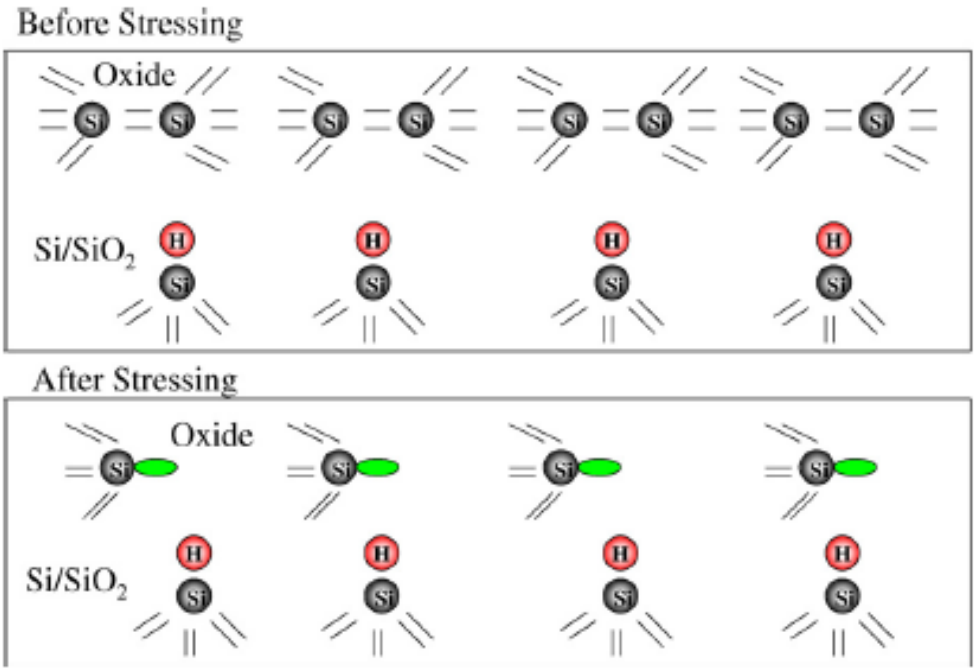

Figure 2-4: Pre and post stressing oxide states

Defect Characterization via EDMR and ESR Techniques

ESR is a powerful tool for analyzing the atomic structure of semiconductor materials. ESR works by utilizing the slight energy differences between the different spin states an electron can occupy in a single orbital. It is sensitive to any defects which have an odd number of electrons in an orbital. This includes almost all defects except for those which may capture or release two electrons instead of just one.

ESR requires a very large magnetic field and measures the absorption and reflection of microwave energy inside a microwave cavity. This cavity is designed to hold a standing wave. The very large magnetic field aligns the electron spins and the microwave radiation is meant to flip the spins when the energy of the microwaves exactly matches the energy difference between the spin states as seen in Figure 2-5. (Doss, 2014)

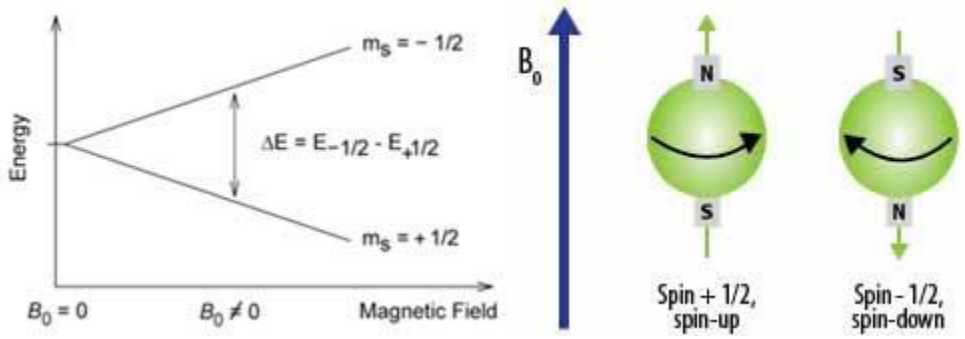

Figure 2-5: Energy difference between spin states

In the simplest of cases, when the energy difference between the two spin states exactly matches the photon energy given by the equation

$$\Delta E = h\nu = g\beta B$$

where $h\nu$ is the energy of the microwave photons, g is the zero crossing of the first derivative of the signal, β is the Bohr magneton, and B is the magnetic field strength, the microwave energy is absorbed by the materials producing a signal. The above image is the simplest case and the energy difference between spin states can be given by a more complex expression.

This method is very good at finding all of the defects that you are looking for, however it can also find the defects that are not as important. For example, if the defects at the oxide semiconductor-interface are the ones that are most limiting the performance of the device, it would be useful to find only these defects and neglect the defects in the larger bulk materials which do not affect the performance. There is a technique that can accomplish this task called EDMR.

EDMR is a very powerful tool that can utilize lower magnetic fields than ESR. (Koichi, 2001) EDMR measures the change in recombination currents as a result of the electron resonance instead of microwave energy absorption. The current occurs in the active region of the devices and so only the relevant defects in those active regions are detected by this technique.

EDMR works by measuring the Spin Dependent Recombination (SDR) effects during an electron resonance experiment. Kaplan, Solomon, and Mott (1978) described this effect as an electron and hole forming a bound pair in either a singlet or triplet state. The current theory is that when a single electron in a deep level defect undergoes resonance and changes its spin, an electron from the conduction band, that previously had the same spin and therefore could not enter the defect due to the Pauli Exclusion Principle, is now capable of entering that defect. The electron then sits in that trap until a hole comes along to recombine with it or vice versa. This recombination current is measured under a quasi-static magnetic field in order to determine when resonance occurs. The resonance conditions for ESR and EDMR match exactly, making EDMR a very useful tool when searching for defects in specific active regions of devices.

Low Field/Zero Field Measurements in Full Devices

Another way to measure EDMR experiments is spin dependent tunneling (SDT) through a capacitor. When the magnetic field applied to a Si-SiC:H capacitor is swept from a negative

polarity across the “zero field” to a positive polarity there is a clear zero field SDT signal that can be measured. The zero field measurement only requires low magnetic fields of about -150 Gauss to 150 Gauss and does not require any microwave irradiation. This lower field requirement and lack of electromagnetic energy makes such a spectrometer significantly cheaper and smaller than a traditional ESR spectrometer. (Cochrane, 2012) This zero-field SDT measurement only detects defects at or around the dielectric layer of the capacitor which ensures that the signal is only coming from the performance inhibiting defects that cause leakage currents in fully processed devices allowing for a better understanding of the defects associated with problems like TDDB and Variable Range Hopping. (Cochrane, 2012) These zero field measurements also detect hyperfine interactions from local magnetic nuclei which aids in the characterization and classification of defects. (Cochrane, Lenahan, 2013)

Helmholtz Coil Design

All magnetic resonance related measurements naturally require the presence of a very well controlled magnetic field to align the electron spins before resonance can take place. It is important that the field be uniform to avoid any effects of a magnetic field gradient which will degrade the measurements. Helmholtz coils offer a method to apply a highly uniform magnetic field of a desired strength across a given volume making them ideal for electron resonance experiments.

EDMR experiments only need a field strength of about 150 Gauss so using a traditional ESR electromagnet capable of achieving several thousand Gauss would be a waste of resources. It is possible to make a custom built Helmholtz coil spectrometer that exactly matches the desired experimental parameters and supply a precisely controllable, highly uniform, comparatively low

magnetic field. These custom built devices are orders of magnitude less expensive than the large magnets used in ESR measurements.

Helmholtz coils must be set up in a very precise manner with many interdependent dimensions to ensure field uniformity. For example, it is important that the distance between the coils be exactly the radius of the coils. Rautela (2011) outlined a lot of these design parameters in his paper on Helmholtz coil design. The most important part of the magnet design is to ensure that the desired field can be attained. The magnetic field supplied by Helmholtz coils in the middle of the coils at the axis of symmetry is defined by the equation:

$$B = 0.899 \frac{N I}{R}$$

where B is the magnetic field in Gauss, N is the number of turns on one side of the coils, and R is the radius of the coils in centimeters. (Rautela et al, 2011) With several sets of progressively larger coils one must calculate the field produced by each coil and add them as vectors. This is very easy because all of the vectors are aligned in the same direction so it reduces to scalar addition.

There are several ways to ensure that the magnetic field produced by the coils is uniform. One of these ways is to introduce a very large outer coil into the design such that the entire apparatus is composed of several progressively larger Helmholtz coils. The large outer coils provide good field uniformity and reduce the radial gradient of the magnetic field in the experimental region. The higher homogeneity of the field allows for better measurements to be taken during the EDMR experiments with less noise. (Wang et al, 2002)

With the knowledge gained by going through the literature on the topic, the decision was made to start by designing and building a low field Helmholtz coil EDMR spectrometer to be used for low field and zero field measurements.

Chapter 3

Helmholtz Coil Design Process

MATLAB Code

In order to determine the length of wire and the size of the coils required to produce a field strength of about 150 Gauss, a MATLAB script was used to calculate all the pertinent information. This script is found in Appendix A. This script was run several times with different input parameters to calculate what size of coils and number of turns would provide the best field. The code took into account such things as the location of the coils, the radius of the coils, the diameter of the wire, and the desired number of turns and calculated the field that could be achieved by the available power source, the length of the wire, the resistance of that length, and the depth of each coil. The radius of each coil was preset by the thickness of materials that were to be used because of the requirement that the radius be exactly the lateral distance between the coils as seen in Figure 3-1. (Rautela et al, 2011)

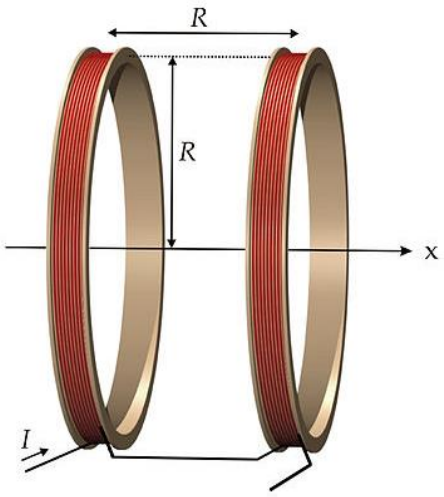

Figure 3-1: Helmholtz Coil Locations

If any of the output parameters were unsatisfactory such as a very thick wire diameter resulting in an unachievable depth of each coil, the script was run again with a new set of input parameters until the design was optimized. The code was designed to optimize the power output of the 100 Watt power source by ensuring that the resistance of the wire would allow for the 2 ampere current draw at 50 volts. This means that the wire should have a resistance of about 20-25 ohms. It was decided that the resistance should be cut down a little, taking into account any unforeseen additions to the resistance by electrical contacts or variations from the ideal resistivity of the copper wire to ensure that the maximum current can be drawn because the generated field depends on current through the wires, not on the voltage. (Rautela et al, 2011)

The final design of the magnet after several iterations of the script was a 20 AWG enamel coated copper magnet wire with 600 turns distributed with 50% of the turns on the first coil, 25% on the second, and 25% on the outer coil. The field achievable by this magnet was 145 Gauss. The field could have been higher if the coils had been placed closer together but it was decided that a larger gap of around 1.5 inches between the innermost coils would allow for the most flexibility and versatility of this magnet's applications. It was designed for use on several projects, some of which require large experimental apparatuses which would require the 1.5 inch spacing.

CAD Modeling

Once the numerical analysis of the magnet was completed, CAD modeling began. The magnet had to be designed for manufacturing so as to ensure that it could be easily made and built once the model had been drawn up. Each piece had to be separately made in Autodesk Inventor and transferred over to a drawing file for cutting out of sheet metal. The CAD model of the magnet which can be seen in Appendix B took into account everything from wire paths to

locations to make electrical connections to the stability of the overall design. One of the limitations on the design was the experimental tool used to hold the samples in place and create electrical connections called a "T" as seen in Figure 3-2. The T's are printed circuit boards (PCBs)where the electrical contacts are located in the central region of the spectrometer where the magnetic field is strongest and most uniform.

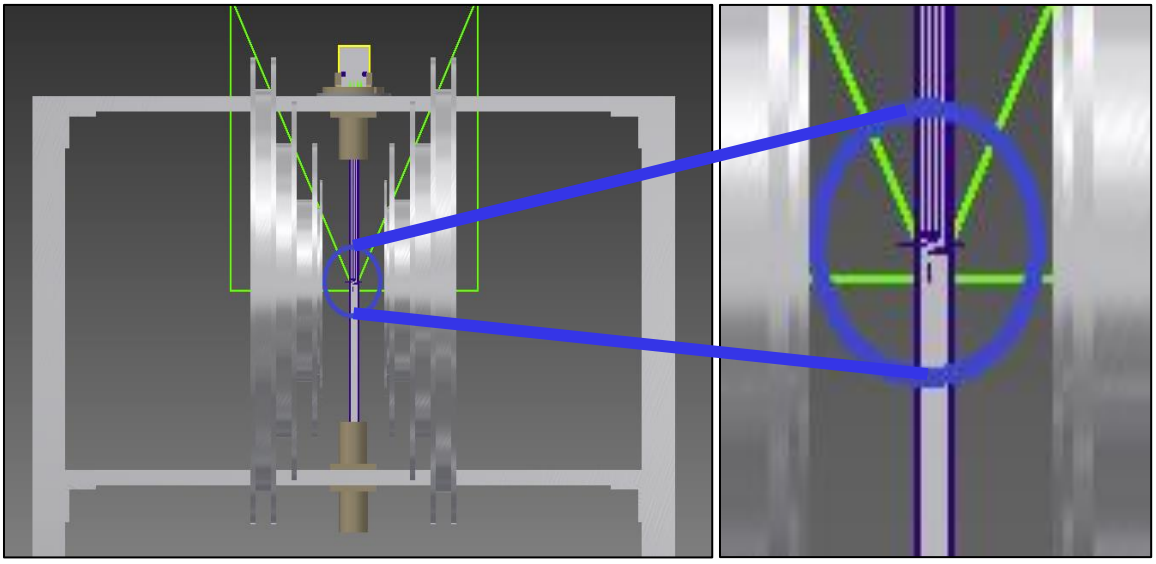

Figure 3-2: Magnet Assembly with T-holder

These "T" holders had been made previously for use in a larger field custom built spectrometer and so the design had to accommodate these older parts. Small changes to the ideal model from the MATLAB script had to be made to ensure that no support structures interfered with the electrical components of the coils. This meant removing some of the turns from the middle coil to accommodate the structural crossbar that would hold everything together. The crossbars also provided locations for BNC attachments to be integrated into the final design outside of the main coils. These connections were to be used for connecting the two sides of the coils together as well as connecting the coils to the main power source.

The main structural support for the design were T-Bars (not to be confused with the PCB T-holders) which, given their large second moment of area, would provide a steady base without

fear of the legs buckling under the mechanical load of the weight of the Helmholtz coils. It was important to ensure a high moment of area to prevent buckling because the entire design had to be made of aluminum to prevent any unwanted fluctuations in the magnetic field from ferromagnetic materials such as ferritic steel. It was also important to use only brass screws and fittings that wouldn't interfere with the magnetic field produced by the coils.

Another constraint that required raising the height of the coils and lengthening the T-Bar legs was the use of the "Cold Finger", a small glass vacuum tube that must be inserted into the experimental region to perform variable temperature experiments. Enough room had to be allowed underneath the lower structural crossbar to slide the cold finger into place so it could be screwed onto the frame via a threaded attachment point.

Building Techniques

Fabrication of Structural Frame

The main structural frame had to be made of aluminum in order to prevent any interference to the magnetic field from ferritic steel or other ferromagnetic materials. These parts were mostly cut on the Waterjet precision cutter in the Learning Factor at the Engineering Services Building in the west section of campus. The smaller pieces such as the legs and the brackets were all milled by hand on the 3-axis milling machines also at the Learning Factory. The plastic pieces such as the threaded attachment points and the variable angle T-holder were made using the plastic additive manufacturing machines at the learning factory and then altered by hand via threading die to ensure a proper fit.

Each piece was then de-burred, sandblasted, beveled, and polished using a *Scotch-Brite* pad to ensure a clean finish without sharp edges that could damage the coating on the wires during the winding of the coils. Once the pieces were cleaned up, the entire frame assembly was constructed to ensure a proper fit. Only brass screws and fittings could be used in the

construction process to ensure that there was no influence of the magnetic field by ferromagnetic parts that could affect the uniformity of the field.

Spun by hand

Wiring the magnet required that the number of turns on each side of the coil match exactly to prevent any gradient in the magnetic field at the center of the experimental region. In order to ensure this, two people had to take the time to wind the coil from a spool by hand counting each turn as it was wound. The basic process involved one person spinning the metal frame in their hands while the other kept tension in the spool of wire to keep a tight wind. The wire could not be simply spun around a stationary coil because such a process led to twisting and subsequently fatiguing of the wire. This fatigue led to broken wires which would be considered a fatal flaw for the magnet. The winding process took several hours to complete each set of coils and was not very repeatable so an alternative had to be found for future builds and re-windings.

Spun on ring stand

The solution to the problem of spinning the coils by hand was to put the coil onto a ring stand (held horizontally) in the laboratory. This allowed for a much faster spinning of the coils and also a much tighter wind. The tighter wind meant a much more uniform distribution of the wires throughout the coil which gives a more uniform magnetic field, and the faster spinning meant that instead of several hours of winding each set of coils, the entire magnet could be wound in the space of about 3 hours.

Problems Encountered and Fixes

There were several problems that were encountered during the building of the Helmholtz coils that had to be addressed and solved before a usable prototype could be considered finished. The first problem that was encountered occurred during the initial building of the frame. Some of

the pieces didn't fit together properly. This was attributed to the waterjet cutter at the Learning Factory. At some point during the cutting process, the cutting head bumped into the wall of the cutting bed and knocked it out of alignment so new parts had to be cut to fit into the design. Once these new parts, using the same drawings as before, were cut and finished via the methods stated in the previous section, they were integrated into the main frame and all of the parts then fit together very nicely.

The second big problem had to do with the building process. Each of the coils had to be wound separately and the coils had to be wound from the outermost to the innermost coils so the wire could be fed through the paths cut into the plates. This at first seemed like it would not be difficult but the force exerted by the previously wound coils proved to be far more than originally anticipated. As such, when the next coil sections were added, the previously wound sections had to be clamped tightly to ensure that the force exerted by the wire did not push the plates apart which could lead to wires getting pinched and losing their insulating coating. Once C-clamps were put into place, the screws that held the coils together could then be removed in order to put the next section on. This process had to be repeated for every new section of the coils and it was found that this fix was satisfactory to hold the coils together and prevent the wires from pushing the plates apart.

After the first winding of all the coils, it was discovered that although the edges of the aluminum plates had been deburred and smoothed, there was still a significant amount of pressure on the wire's insulation which cut through the enamel and created an electrical short between the aluminum frame and the conductive wires. This would also be considered a fatal flaw in a prototype as the magnetic field produced could not be considered reliable and repeatable if there are other paths for the current to travel other than the desired wire paths.

The first attempt to fix this problem was forcing insulating rubber shrink tubing into the wire paths through the plates where most of the shorts were thought to be. This however was an

unsatisfactory solution because the pressure on the wire at these locations prevented the insulating tubing from reaching the locations where the shorts occurred. The second attempt to fix the shorting problem was to unwind the coils and insert the rubber shrink tubing on the wire before placing it against the metal frame. This worked at first but the stresses applied to the wires during the winding process eventually scraped the rubber tubing against the edges of the metal frame with enough force to cut through and cause another short.

After these two attempts to prevent any electrical contacts between the wire in the coils and the aluminum frame, a new approach had to be taken. The entire assembly was taken apart and re-sandblasted in an attempt to soften any remaining sharp edges. This sandblasting helped a very small amount but the best solution came from filleting the edges where the wires passed through the plates. These small fillets were made by a handheld drill to create a less drastic turning of the wires which lessened the wire scraping against the edges of the frame. This filleting almost solved the shorting problem but other steps still had to be taken.

Several test sections of wire were made to be intentionally scraped against the metal edges of the plates to see which would provide the most robust and reliable solution to insulating the wires. The first solution tested was to wrap the enamel coated wire in a rubber shrink tube but this configuration failed after several scrapes against the metal edges. The next configuration involved using a plastic coated wire as the section that would be placed against the metal edges. This plastic coated wire would then be soldered to the enamel coated wire at a location inside the frames and wrapped in a rubber shrink tube where there would be little to no stress on the joint. This solution prevented any shorting from occurring but the soldered joint took up valuable space inside the frame where the wires had to be wound. It was determined that this solution was good for insulating but would not be viable due to the volume of the joint.

The final configuration involved removing the strong plastic coating from one of the thicker gauge wires in the laboratory and utilizing this insulating layer as a secondary layer over

the enamel coating of the magnet wire. This configuration was similar to wrapping the wire in the rubber shrink tubing but the plastic insulation was much stronger and could be scraped against the metal edges for at least 100 cycles without failure. It was determined that 100 cycles at a very high load would be a good test as this was significantly higher than the expected loads during the winding process as experienced in the previous build. This solution offered the best insulating properties with the smallest amount of volume taken up (because the large solder joint was located outside the coils) and so was chosen as the preferred method of preventing the shorting problem.

This final fix entirely solved the problems associated with electrical shorts to the metal frame and no electrical contacts between the wire and the aluminum frame have been discovered since the application of the fix stated above. With this problem out of the way it was then possible to begin validating and calibrating this spectrometer by using it to carry out zero-field measurement experiments on “standard” silicon carbide transistor samples that had already been well characterized.

Chapter 4

Design Validation

Zero-Field Signal

The first experiment that was carried out on the new Helmholtz coil spectrometer was a zero-field measurement on an already well characterized SiC transistor. Before initial zero-field measurements could be taken, it was necessary to design a measuring apparatus that could determine the amplitude and frequency of the current in the modulation coils which couldn't be assumed as purely resistive due to a small inductance in the coils. Furthermore, the ideal measuring tool for a high frequency sinusoidal signal is an oscilloscope but an oscilloscope can only directly measure voltage, not current. It was impossible to know the current through the coils based on the voltage drop across them due to the inductance. This issue was circumvented by introducing an extra section to the circuit known as a "mod box" which is essentially a small resistor placed in series with the coils so the voltage across can be measured. The mod-box utilizes the linear voltage-current characteristics of a resistor to determine the current. To make things very easy, a 10 watt 1Ω resistor was used so the voltage to Ampere conversion was 1 to 1.

There is still a problem with the modulation coils where the exact amplitude of the modulating field cannot be calculated due to electromagnetic energy being absorbed by the aluminum frame. The modulation coils introduce a very rapidly changing magnetic field which induces current loops in the aluminum that will dampen the field experienced at the center of the experimental region. This problem could be fixed by replacing the innermost aluminum plates with plastic but it seemed more advantageous to utilize the heat conducting properties of the aluminum and simply ramp up the currents in the modulation coils rather than dismantle the apparatus again. This was accomplished by amplifying the signal with an audio amplifier. The

hope in the future is to measure the field exactly using a Gaussmeter which directly measures the field instead of assuming the field strength based on current input. The mod-box design and modulation coil circuit can be seen in Figure 4-1.

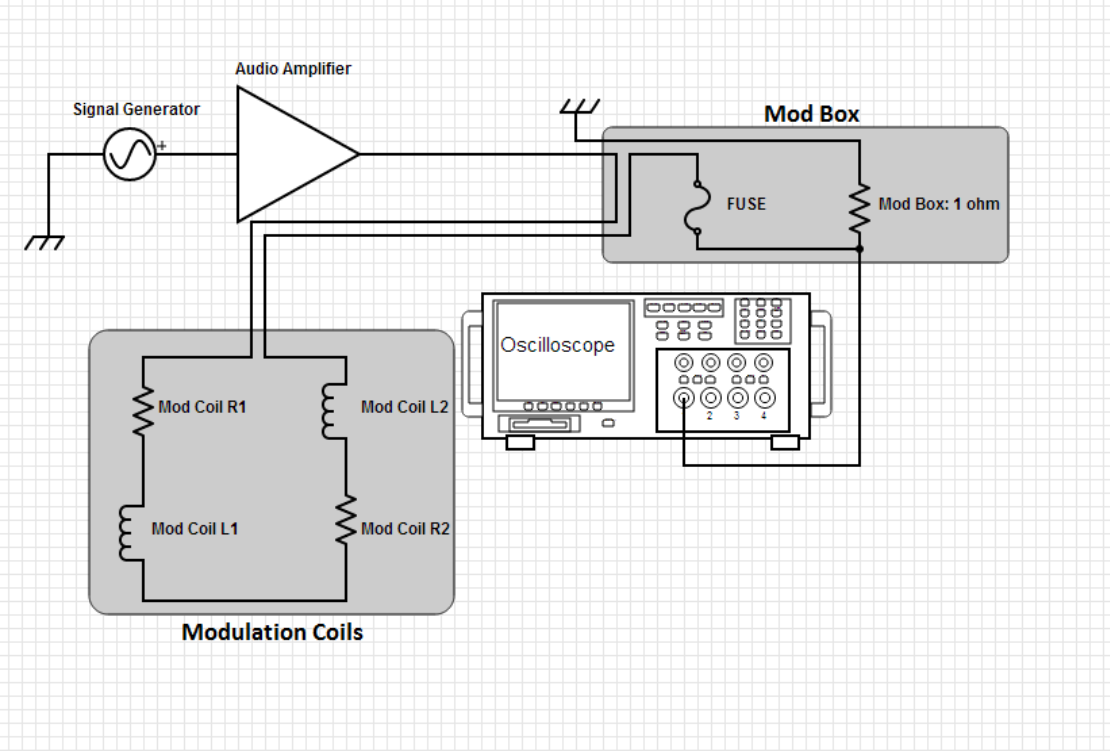

Figure 4-1: Modulation Coil Circuit Diagram

Once the current through the modulation coils was determined, zero-field experiments were carried out where the magnetic field from the large main coils was gradually swept from -75 Gauss through the zero field mark to 75 Gauss. The modulation coils were given a 6 volt peak-to-peak signal at 1.3 kHz to provide an oscillating magnetic field of about 6 gauss peak-to-peak. This oscillation brings the system in and out of resonance quickly. A lock in amplifier boosts signals matching the frequency of the modulation coils which is the exact frequency of the SDT signal. This frequency based detection enhances the signal-to-noise ratio of the spectrometer. The data was further enhanced by a signal averager to boost the signal-to-noise ratio.

Without any way of transferring the data from the signal averager to another format, a picture was taken of the signal with a smartphone camera. An example of one of the first zero field signals from a silicon carbide MOSFET is shown below in Figure 4-2. This signal is the first derivative of a broadened impulse function with the peak of the current signal occurring at the inflection point in the center of the plot around the zero field mark.

Figure 4-2: First Zero Field Resonance Signal

For future experiments, a computer may aid in the data acquisition to allow for more precise measurements. The spectrometer currently utilizes a custom built “bias box” to provide the required biasing voltages to the transistor and to provide a path for the SDT current to the pre-amplifier which then filters and converts the current signal to a voltage signal. This filtered signal is then sent to the lock-in amplifier that also provided the modulation frequency, which detects any signals at the frequency of interest. This signal is then sent to a signal averager to be displayed to the screen. There is currently no computer or other digital means to measure and analyze the data from the transistor but this is being worked on and hopefully a computer will be available soon.

Chapter 5

Results and Discussions

The experiments that were carried out during the design validation were continued with more measurements taken on the SiC transistor. As the instrument was used more and the general settings of the electrical measuring devices like the filters and sensitivities on the preamplifier and the lock in amplifier were optimized, better zero-field signals with a much higher signal-to-noise ratio were observed using this spectrometer.

The initial purpose of this spectrometer was for use on low dielectric constant materials as used in gate dielectric stacks in MOSFETs, and this will still be done. These measurements on the silicon carbide transistor were carried out to better understand both the transistor and the spectrometer. The large signal came from the spike in the recombination current when the electrons in the defects in the active region of the transistor flipped their spins. The electrons flipped spins because of the change in the polarity of the magnetic field when it is swept from a negative direction, through the zero field mark, and finally through to a positive direction. This spin flipping in the defect electrons caused previously unallowed transitions of free electrons with the same spin as that of the electrons in the defects (due to the Pauli Exclusion Principle) to become allowed as the two electrons involved in the process had different spins. Continuing the work on silicon carbide seemed like a good choice because although it is not a low k material it is good to get a better understanding of the measurements and the instrument on samples which have already been fairly well characterized.

The large signals measured from the sample are likely from defects similar to those discovered in the last study of this sample. Prior to the construction of this low-field/zero-field spectrometer the transistor device was measured under EPR and it was determined by Pomorski (2013), that the defects that were causing the largest amount of leakage current through the device

was likely a hydrogen atoms bonded to either a silicon or carbon and that it could be determined which atom it was likely bonded to by analyzing the band gap of the material. Most of my project focused on the design and construction of the spectrometer and getting this data was not necessarily anticipated when starting this project. I would like to take more time to analyze this material as well as the low dielectric constant materials to get a better understanding of both materials. The best zero-field signal from the silicon carbide transistor measured can be seen in Figure 5-1.

Figure 5-1: Silicon Carbide Transistor Zero-Field Signal

Other experiments have been carried out on some cadmium telluride solar cells but the experimental setup and measurement settings are still being worked out to get good measurements. The measurements that have been made on the silicon carbide show a lot of promise and show that this instrument will be a good tool to use on the new uncharacterized low dielectric constant materials.

Chapter 6

Conclusions

The magnet was declared to be a success as it proved to be uniform for good zero field EDMR measurements. This magnet is the second of its kind in Dr. Lenahan's lab and it is believed that there are very few, if any, like it in other labs. The purpose of this magnet is to perform low-field and zero-field EDMR on low-k dielectric materials and CdTe solar cells. For the purpose of validation the magnet was used for EDMR on SiC transistors with known zero field signals. The anticipated signals were seen exactly with a very good signal to noise ratio which seems to be better than its predecessor. This signal to noise ratio will be one of this spectrometers greatest assets for future work.

With the completion of the magnet there is now an opportunity to utilize this apparatus, with a few adjustments to the data acquisition technique, to analyze the defects in the low capacitance dielectric materials. Understanding what is causing the problems in these dielectrics could introduce a new wave of faster, smaller, more energy efficient transistors and processors. This new technology will help ensure that Moore's law continues as it has for so long. While it is impossible to know exactly what could come out of understanding these defects, it is certain that this Helmholtz coil EDMR spectrometer is capable of shedding new light in the field of semiconductor spectroscopy.

I look forward to my continued work on this novel, research quality instrument. Over the next few years I hope to use this spectrometer for its original purpose of analyzing low-k transistor devices to better understand the physics taking place inside them and to shed more light on phenomena like TDDB, VRH, and SILC. I have recently accepted an offer of admission to The Graduate School at The Pennsylvania State University where I will be conducting my research on this new high fidelity instrument.

Appendix A

MATLAB Code

```
clear
clc
format short g
% Colin McKay
% Helmholtz Coil Calculations
%
%   This code was written to aid in the design of a cutom built
%   Helmholtz coil spectrometer for use in my senior thesis.
%
%   This code was run itertatively to determine the best wire diameter
%   and number of turns to get a coil that achieves the right field and
%   fits onto the table in the lab.

%% Initial data/Constants
u_0=1.257e-6;               % Permeability (Tesla*meters/amperes)
Voltage=50;                 % Maximum voltage of power source (volts)
Current=2;                  % Maxium current of power source (amperes)
inch_to_meter=.0254;        % Used for conversions between measurments
and calculations (meter/inch)
d=1.5;                      % Size of gap between the coils where
samples are placed (inches)
wdiam=inch_to_meter*.03;    % Wire Diameter (meter)
n=600;                      % number of turns per side of the magnet

%% Locations of coils (based on build style)
% Calculated by adding the thicknesses of the different plates (meters)
X_1=inch_to_meter*(d/2+1/16+1/16+1/8+.5*(3/8));                 % X
Location of first coil
X_2=inch_to_meter*(d/2+1/16+1/16+1/8+3/8+1/8+.5*(3/8));         % X
Location of second coil
X_3=inch_to_meter*(d/2+1/16+1/16+1/8+3/8+1/8+3/8+1/8+.5*(3/8)); % X
Location of third coil

% Coil Locations (inches)
x_1_inch=(X_1/inch_to_meter)
x_2_inch=(X_2/inch_to_meter)
x_3_inch=(X_3/inch_to_meter)

 %% Radius of each Coil
% Calculates the optimal radii for the coils
R_1=2*X_1;      % Radius 1 (meters)
R_2=2*X_2;      % Radius 2 (meters)
R_3=2*X_3;      % Radius 3 (meters)
```

```
%% Coil Design
% The coils have an uneven distribution of turns
percent1=.50;
percent2=.25;
percent3=1-(percent1+percent2);

% Number of turns in each coil
FirstTurns=n*percent1
length1=FirstTurns*2*pi*R_1

SecondTurns=n*percent2
length2=SecondTurns*2*pi*R_2

ThirdTurns=n*percent3
length3=ThirdTurns*2*pi*R_3

%% Calculates the length, resistance, and Voltage
l=2*(length1+length2+length3);  % Length of wire (meters)
Length_ft=l*3.28084  % Converted to feet
rho=1.68e-8;    % Resistivity (ohm*m)
A=pi/4*wdiam^2;    % Area of wire
resistance=rho*l/A      % Resistance of wire (ohms)
Voltage=Current*resistance;


%% Imposing design constraints (power source)
if (Voltage>50)
    Voltage=50
    Current=Voltage/resistance
else
    Current=Current
    Voltage=Voltage
end

%% Calculates depth of wire coils
% the 1.3 term assumes a non-ideal packing density
height1_inches = 1.3*FirstTurns*(wdiam/inch_to_meter)^2/(3/8)
height2_inches = 1.3*SecondTurns*(wdiam/inch_to_meter)^2/(3/8)
height3_inches = 1.3*ThirdTurns*(wdiam/inch_to_meter)^2/(3/8)

% Calculates inner and outer diameters for each coil
First_innerD_inch=2*(R_1/inch_to_meter-height1_inches/2)
First_outerD_inch=2*(R_1/inch_to_meter+height1_inches/2)
Second_innerD_inch=2*(R_2/inch_to_meter-height2_inches/2)
Second_outerD_inch=2*(R_2/inch_to_meter+height2_inches/2)
Third_innerD_inch=2*(R_3/inch_to_meter-height3_inches/2)
Third_outerD_inch=2*(R_3/inch_to_meter+height3_inches/2)

%% Calculating the Field!
B=(4/5)^(3/2)*(u_0*FirstTurns*Current)/R_1+(4/5)^(3/2)*(u_0*SecondTurns
*Current)/R_2+(4/5)^(3/2)*(u_0*ThirdTurns*Current)/R_3;  %(Tesla)
B=B*10000  % (Gauss)
```

Appendix B

AUTODESK Inventor Models and Final Product

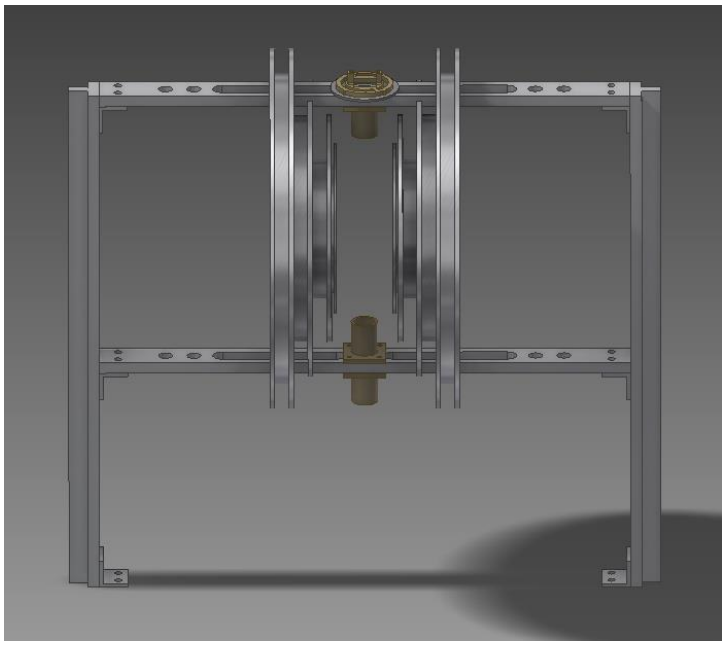

Figure 0-1: Magnet CAD Model Full Assembly

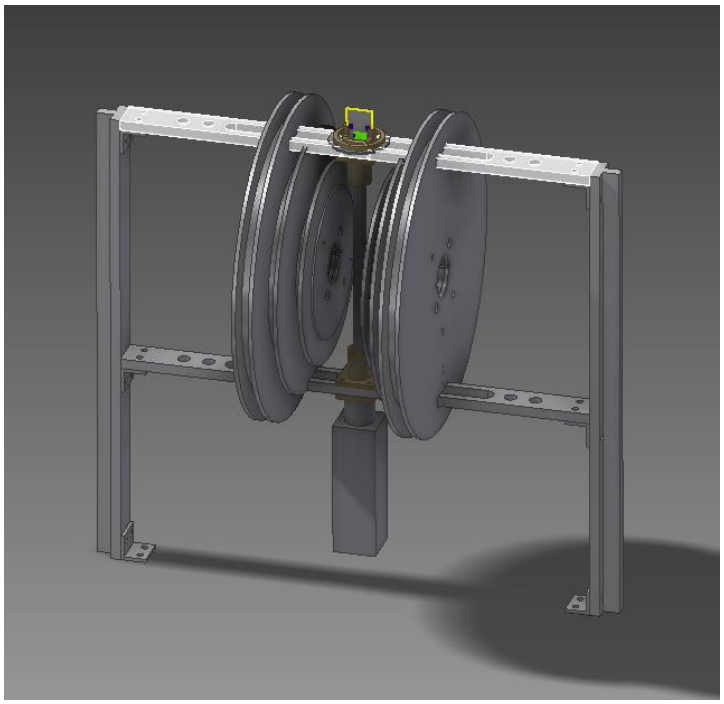

Figure 0-2: Magnet CAD Model Assembly with Cold Finger and T

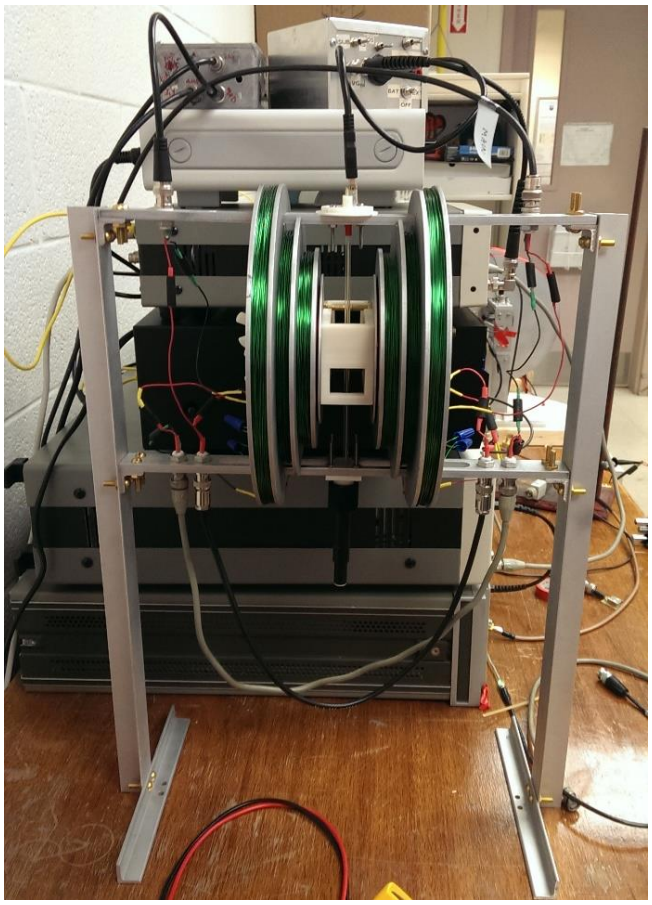

Figure 0-3: Completed Wired Magnet

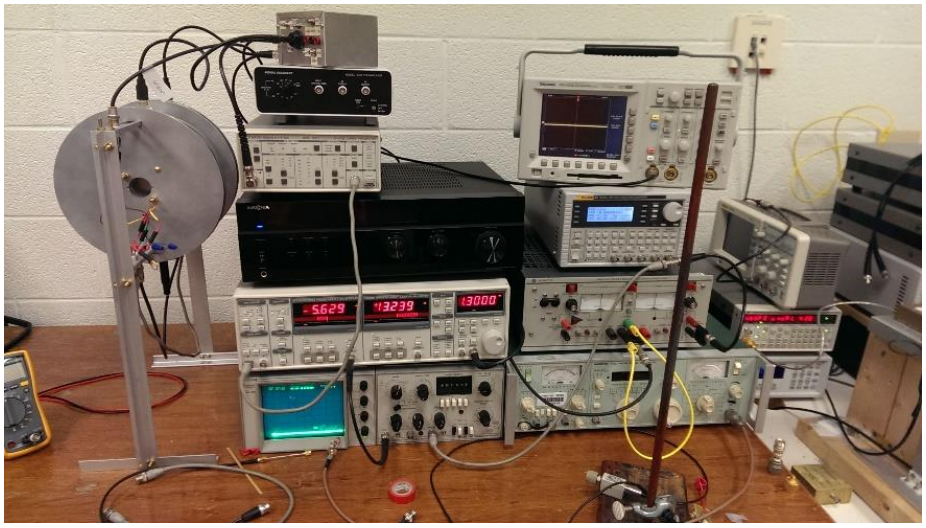

Figure 0-4: Experimental Setup

BIBLIOGRAPHY

1. Bohr, M. (n.d.). Intel's Revolutionary 22 nm Transistor Technology. *Intel's Revolutionary 22 nm Transistor Technology*. Retrieved March 21, 2014, from http://download.intel.com/newsroom/kits/22nm/pdfs/22nm-Details_Presentation.pdf

2. Mott, N. F. (1987). *Conduction in non-crystalline materials*. Oxford: Clarendon Press.

3. Chen, F. (2009). Critical ultra low-k TDDB reliability issues for advanced CMOS technologies. 2009 IEEE International Reliability Physics Symposium (IRPS) (pp. 464-75).

4. McPherson, J. (1998). Comparison of E and 1/E TDDB models for SiO2 under long-term/low-field test conditions. Technical digest - International Electron Devices Meeting, 171-174.

5. Miyazaki, Hiroshi and Kodama, Daisuke and Suzumura, Naohito, (2009) Phenomenological classification of stress-induced leakage current and time-dependent dielectric breakdown mechanism. Journal of Applied Physics, 106, 104103, DOI:http://dx.doi.org/10.1063/1.3259386

6. Lenahan, P.M., "A model for NBTI in nitrided oxide MOSFETs without hydrogen or diffusion," *Reliability Physics Symposium (IRPS), 2010 IEEE International* , vol., no., pp.1086,1090, 2-6 May 2010 doi:10.1109/IRPS.2010.5488669URL: http://ieeexplore.ieee.org/stamp/stamp.jsp?tp=&ar

number=5488669&isnumber=5488659

7. P.M. Lenahan, Deep level defects involved in MOS device instabilities, Microelectronics Reliability, Volume 47, Issue 6, June 2007, Pages 890-898, ISSN 0026-2714, http://dx.doi.org/10.1016/j.microrel.2006.10.016. (http://www.sciencedirect.com/science/article/pii/S0026271406003799)

8. Doss, H. (n.d.). The Future Mind Reader?. Physics Central. Retrieved March 21, 2014, from http://www.physicscentral.com/explore/action/fmri.cfm

9. Kôichi Fukui, Toshiyuki Sato, Hidekatsu Yokoyama, Hiroaki Ohya, Hitoshi Kamada, Resonance-Field Dependence in Electrically Detected Magnetic Resonance: Effects of Exchange Interaction, Journal of Magnetic Resonance, Volume 149, Issue 1, March 2001, Pages 13-21, ISSN 1090-7807, http://dx.doi.org/10.1006/jmre.2000.2277. (http://www.sciencedirect.com/science/article/pii/S1090780700922778)

10. Kaplan, D., Solomon, I., Mott, N. (1978). Explanation of the large spin-dependent recombination effect in semiconductors. Journal de physique. Lettres, 39(4), L51-4.

11. Cochrane, C. J. (2012-10). A means to study reliability based defects in fully processed devices utilizing zero-field spin dependent transport. 2012 IEEE International Integrated Reliability Workshop Final Report (pp. 45-7).

12. Cochrane, C. J. and Lenahan, P. M. (2013). Detection of interfacial Pb centers in Si/SiO2 metal-oxide-semiconducting field-effect transistors via zero-field spin dependent

recombination with observation of precursor pair spin-spin interactions., Applied Physics Letters, 103, 053506, DOI:http://dx.doi.org/10.1063/1.4817264

13. Rautela, R. S.; Bhatt, V.; Sharma, P.; Khushu, S.; Walia, P., "Mathematical approach for designing & development of Helmholtz coil for hyperpolarized Xenon gas used in MRI," *Power Electronics (IICPE), 2010 India International Conference on* , vol., no., pp.1,5, 28-30 Jan. 2011 doi: 10.1109/IICPE.2011.5728083URL: http://ieeexplore.ieee.org/stamp/stamp.jsp?tp=&arnumber=5728083&isnumber=5728055

14. Wang, Jian and She, Shouxian and Zhang, Sijiong. (2002) An improved Helmholtz coil and analysis of its magnetic field homogeneity. Review of Scientific Instruments, 73, 2175-2179, DOI:http://dx.doi.org/10.1063/1.1471352

15. Pomorski, T. A., Bittel, B. C., Cochrane, C. J., Lenahan, P. M., Bielefeld, J., King, S W. (2013). Defects and electronic transport in hydrogenated amorphous SiC films of interest for low dielectric constant back end of the line dielectric systems, Journal of Applied Physics, 114, 074501, DOI:http://dx.doi.org/10.1063/1.4818480

ACADEMIC VITA

Colin McKay
cgmckay@optoinline.net

Education:
The Pennsylvania State University
University Park, Pennsylvania
Schreyer Scholar
Major: Engineering Science (Honors Curriculum)
Graduation: May 2014

Honors and Awards
Schreyer Scholar
Dean's list (FA 10, SP 11, FA 11. SP 12, FA 12, SP 13, FA 13)
Phi Eta Sigma Honors Society

Association Memberships/Activities
Phi Eta Sigma Honors Society
Society of Engineering Science